Supporting Information

Tuning local S coordination environment on Ru single atoms to boost the oxygen evolution reaction

Yiling Ran, Rong Gan, Qin Zhao, Quanlei Ma, Yijing Liao, Yinwei Li, Yi Wang*, Yanwei Wang*, Yan Zhang*
Q. Zhao, Q. L. Ma, Y. J. Liao, Y. Zhang
School of Chemistry, Southwest Jiaotong University, Chengdu, Sichuan 610031, China
Y. L. Ran, R. Gan
School of Life Science and Engineering, Southwest Jiaotong University, Chengdu, Sichuan 610031, China
Y. W. Wang
School of Chemical Engineering, Xuzhou College of Industrial Technology, Xuzhou 221140, Jiangsu, China
Y. L. Ran, Y. Wang
State Key Laboratory of NBC Protection for Civilian, 102205 Beijing, China
Y. W. Li
Laboratory of Quantum Functional Materials Design and Application, School of Physics and Electronic Engineering, Jiangsu Normal University, Xuzhou 221116, China
*Corresponding author:
zyzw@swjtu.edu.cn (Y. Zhang)
wangyw@mail.xzcit.cn (Y. W. Wang)
wangyi2022@tsinghua.org.cn (Y. Wang)

1. Extended X-ray absorption fine structure measurements

Data reduction, data analysis, and EXAFS fitting were performed and analyzed with the Athena and Artemis programs of the Demeter data analysis packages [1]that utilizes the FEFF6 program [2] to fit the EXAFS data. The energy calibration of the sample was conducted through standard and Ru foil, which as a reference was simultaneously measured. A linear function was subtracted from the pre-edge region, then the edge jump was normalized using Athena software. The χ(k) data were isolated by subtracting a smooth, third-order polynomial approximating the absorption background of an isolated atom. The k^2-weighted $\chi(k)$ data were Fourier transformed after applying a HanFeng window function (Δk = 1.0). For EXAFS modeling, The global amplitude EXAFS (CN, R, σ^2 and ΔE_0) were obtained by nonlinear fitting, with least-squares refinement, of the EXAFS equation to the Fourier-transformed data in R-space, using Artemis software, EXAFS of the Ru foil are fitted and the obtained amplitude reduction factor S_0^2 value (0.756) was set in the EXAFS analysis to determine the coordination numbers (CNs) in sample.

2. Density functional theory calculation

Based on density functional theory (DFT), all spin-polarized first-principles calculations were conducted using the Vienna Ab initio Simulation Package (VASP). The electro-ion interactions were described using the projector-augmented wave (PAW) pseudopotentials. The exchange-correlation interactions were expressed using the generalized gradient approximation (GGA) as formulated by Perdew-Burke-Ernzerhof (PBE). To ensure the accuracy of the results, a plane wave with a cutoff energy of 500 eV was utilized to describe the electron wave function. A convergence criterion of 0.03 eV/Å was applied for the minimum force during geometric optimization. A p (2 × 2) supercell with a 12-layer slab consisting of 96 atoms for NiS_2 (100) was modeled, and a 2 × 2 × 1 k-point grid was employed for Brillouin zone sampling during structural optimization.

The formation energies of Ru-doped configurations were calculated using the following equation[3]:

$$E_f = E_{tot} - E_{vac} - E_{Ru} \quad \text{(S1)}$$

where E_{tot} represents the total energy of NiS_2 with Ru-doped metal atoms, E_{vac} is the total energy for NiS_2 with S/Ni vacancy, and E_{Ru} is the energy of one metal atom in its bulk phase.

In alkaline media, the four-electron OER could be described as:

$$OH^- + * \rightarrow OH^* + e^- \quad \text{(S2)}$$

$$OH^* + OH^- \rightarrow O^* + e^- + H_2O \quad \text{(S3)}$$

$$O^* + OH^- \rightarrow OOH^* + e^- \quad \text{(S4)}$$

$$OOH^* + OH^- \rightarrow O_2 + H_2O + e^- \quad \text{(S5)}$$

In these equations, * denotes the catalyst slab The Gibbs free energies for the adsorption of intermediate species (OOH*, O*, and OH*) can be calculated using the following equations:

$$\Delta G = \Delta E + \Delta ZPE - T\Delta S \quad \text{(S6)}$$

The values of $\Delta ZPE - T\Delta S$ for the intermediates were computed using the VASPKIT program[4].

3. Supplementary Figures and Tables

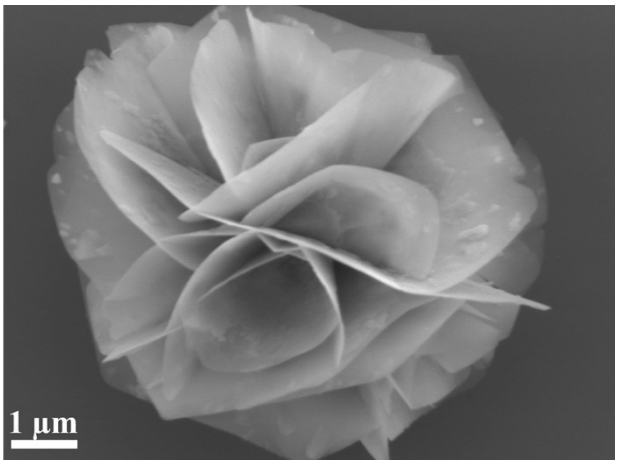

Figure S1. SEM image of Ni precursors.

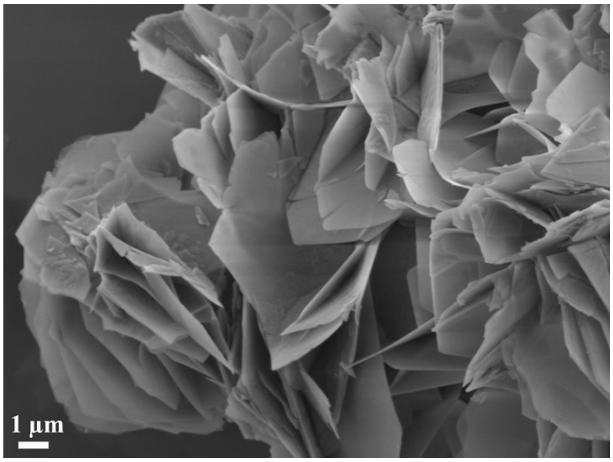

Figure S2. SEM image of $Ni(OH)_2$.

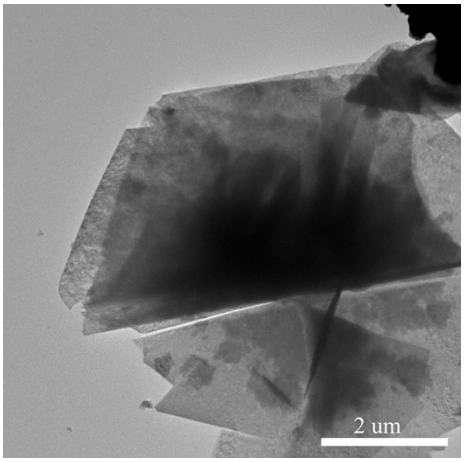

Figure S3. TEM image of $Ni(OH)_2$.

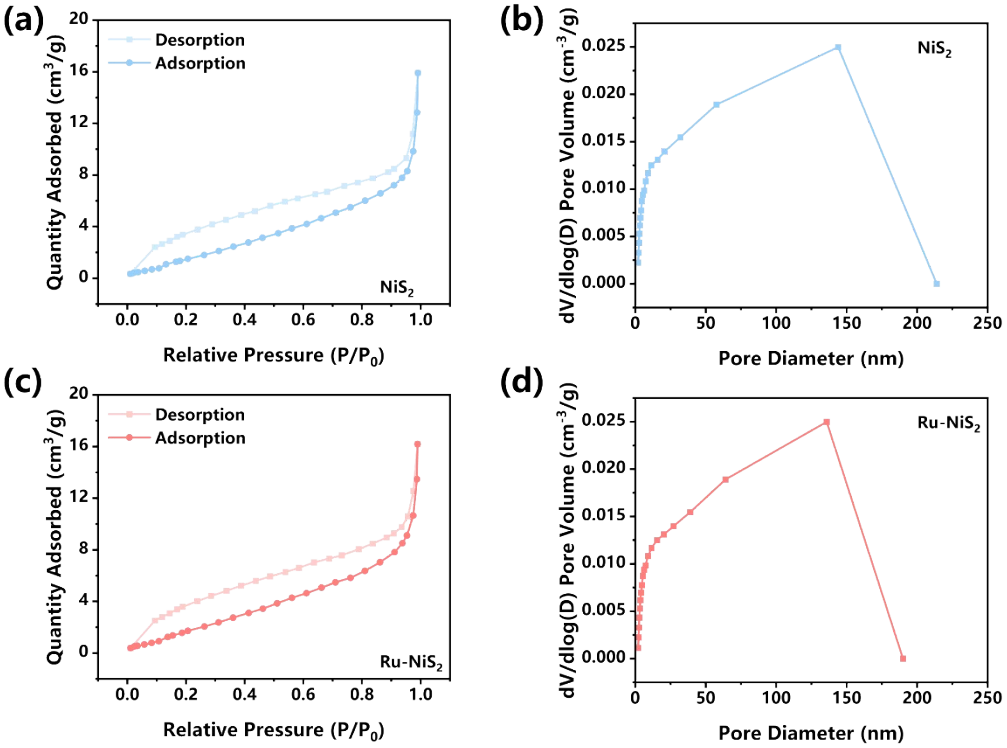

Figure S4. N_2 adsorption/desorption isotherms of (a)NiS_2 and (c) Ru-NiS_2. The corresponding pore size distribution of (b) NiS_2 and (d) Ru-NiS_2.

Table S1. Specific surface area and pore size of Ru-NiS_2 and NiS_2.

Sample	Specific surface area (m^2/g)	pore size (nm)
Ru-NiS_2	9.60	136
NiS_2	10.14	144

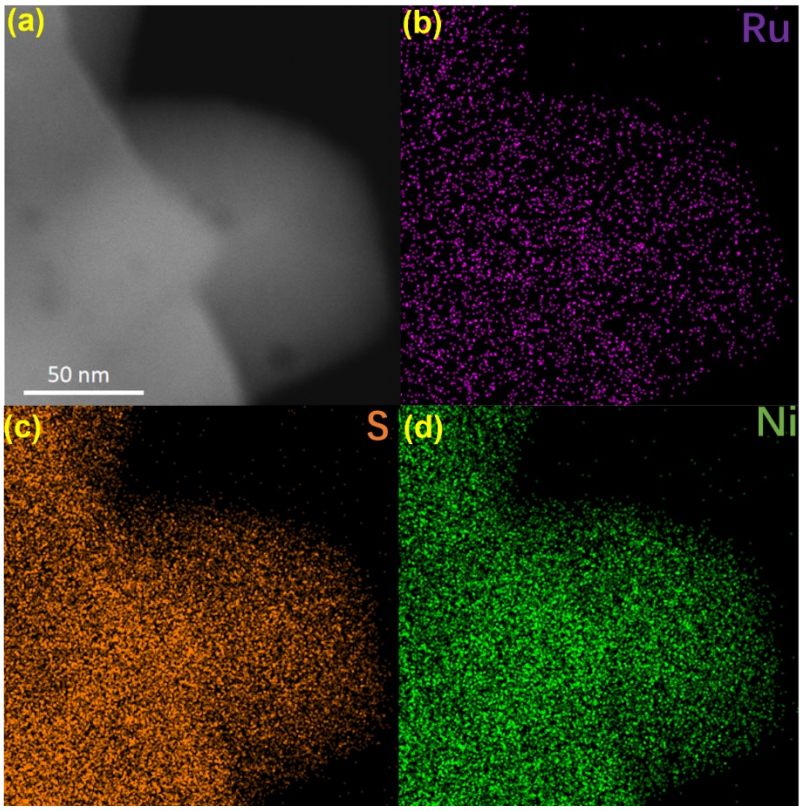

Figure S5. EDS elements mapping of Ru-NiS_2.

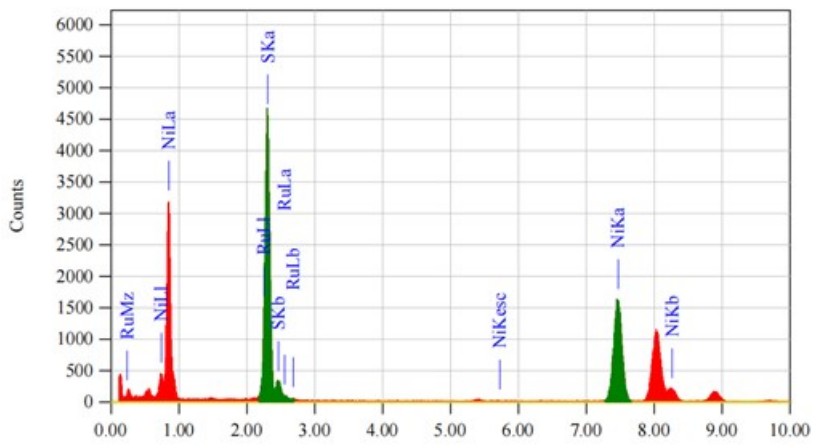

Figure S6. EDS spectrum of Ru-NiS_2.

Table S2. Atom ratio for Ru-NiS_2.

Sample	Elements	Atom percentage (%)
Ru-NiS_2	Ru	0.82
	Ni	65.97
	S	33.21

Table S3. ICP-OES spectrum of Ru-NiS_2.

Sample	**Elements**	**Weight percentage (%)**
Ru-NiS_2	Ru	0.198
	Ni	37.80
	S	62

Table S4. EXAFS fitting parameters at the Ru K–edge for various samples.

Sample	Shell	CN[a]	R(Å)[b]	σ^2(Å^2)[c]	ΔE_0(eV)[d]	*R* factor
Ru foil	Ru-Ru	12*	2.67±0.01	0.0029	1.8	0.0058
RuO_2	Ru-O	6.0±0.6	1.96±0.01	0.0011	7.6	0.0195
	Ru-Ru	10.2±3.1	3.14±0.01	0.0101	5.0	
	Ru-Ru	7.0±0.8	3.58±0.01	0.0025	10.1	
Ru sample	Ru-O	1.2±0.3	2.05±0.01	0.0023	-10.4	0.0196
	Ru-S	5.0±0.4	2.39±0.01	0.0028	7.5	

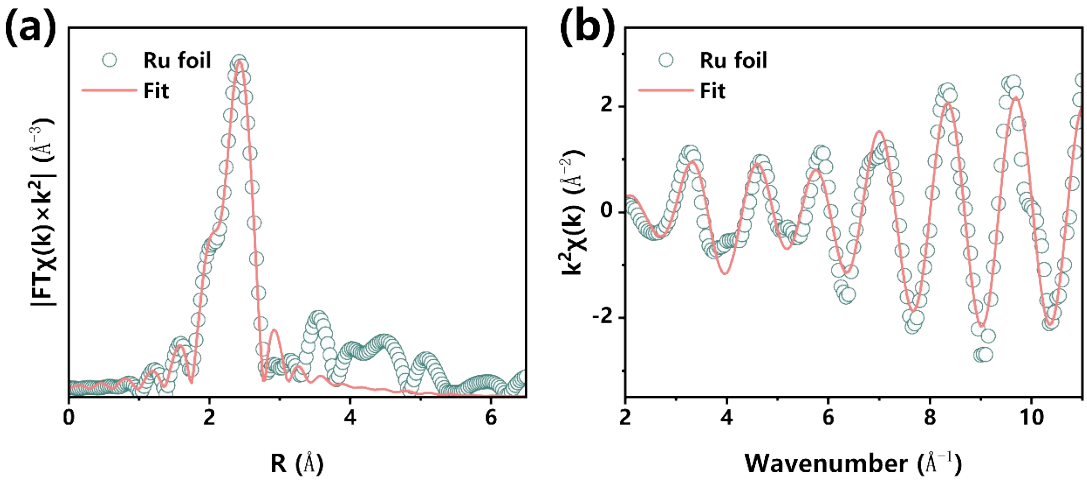

Figure S7. (a) EXAFS fitting results and optimized models for Ru foil at R space. (b) WT for k^2-weighted signals for Ru foil.

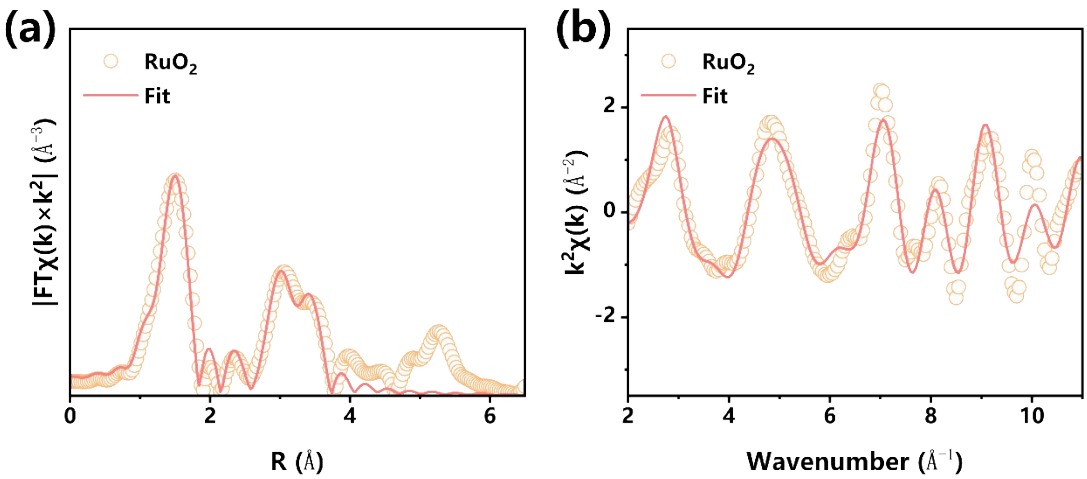

Figure S8. (a) EXAFS fitting results and optimized models for RuO_2 at R space. (b) WT for k^2-weighted signals for RuO_2.

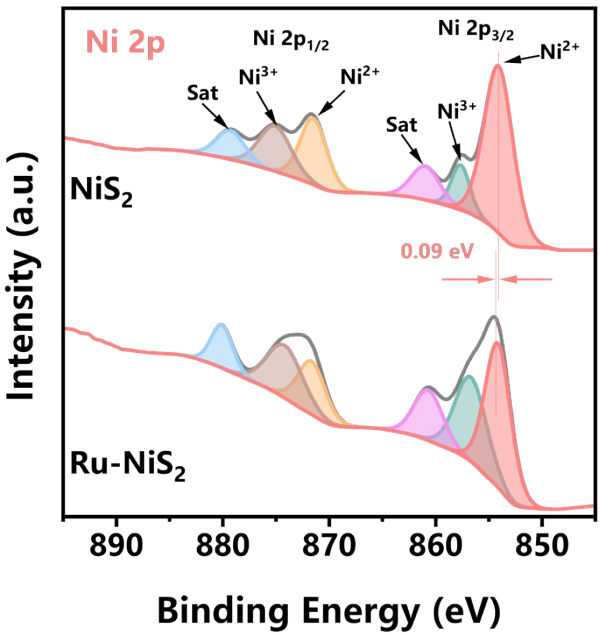

Figure S9. XPS spectra of Ni 2p states in NiS_2 and Ru-NiS_2 samples.

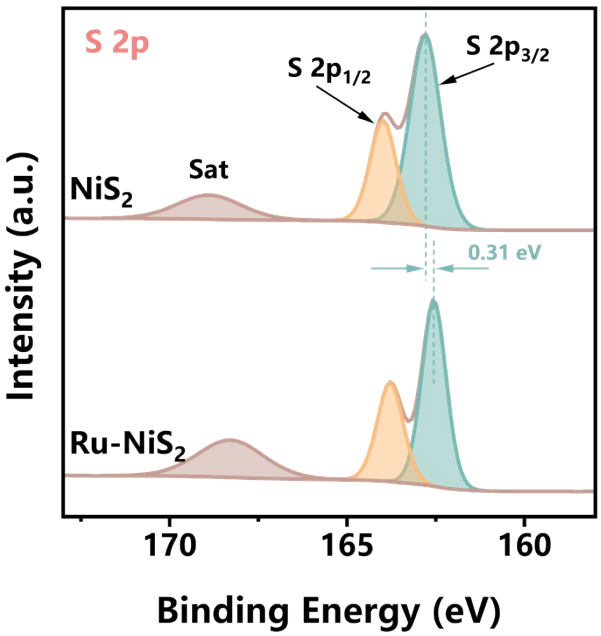

Figure S10. XPS spectra of S 2p states in NiS_2 and Ru-NiS_2 samples.

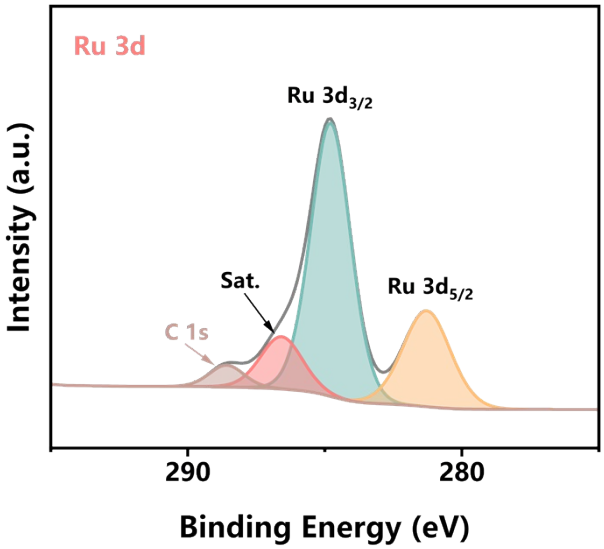

Figure S11. XPS spectra of Ru 3d states in Ru-NiS_2 samples.

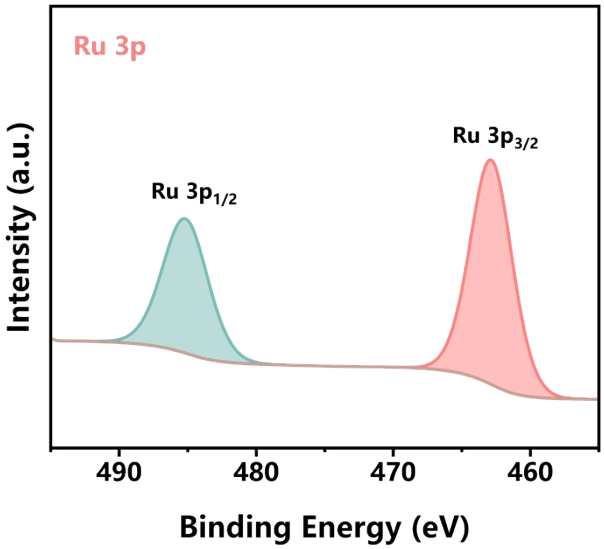

Figure S12. XPS spectra of Ru 3p states in Ru-NiS_2 samples.

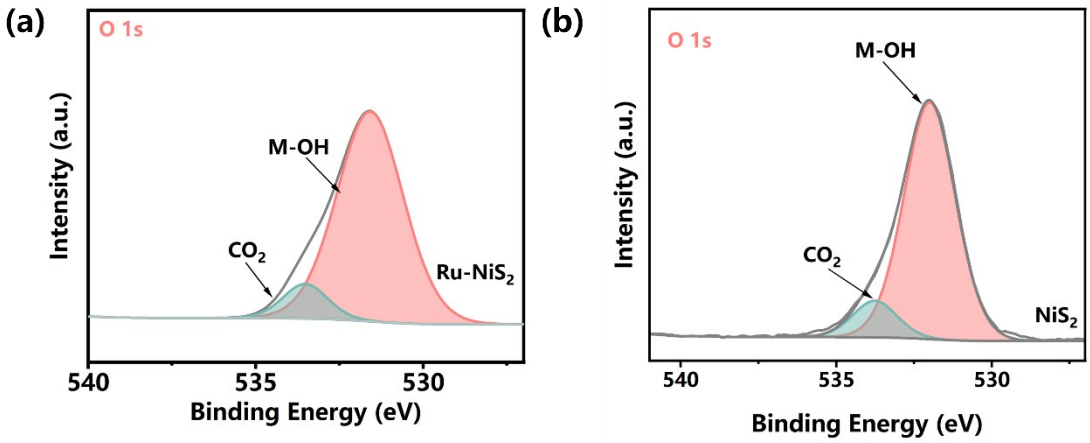

Figure S13. O 1s XPS spectrum of a) Ru-NiS_2 and b) NiS_2.

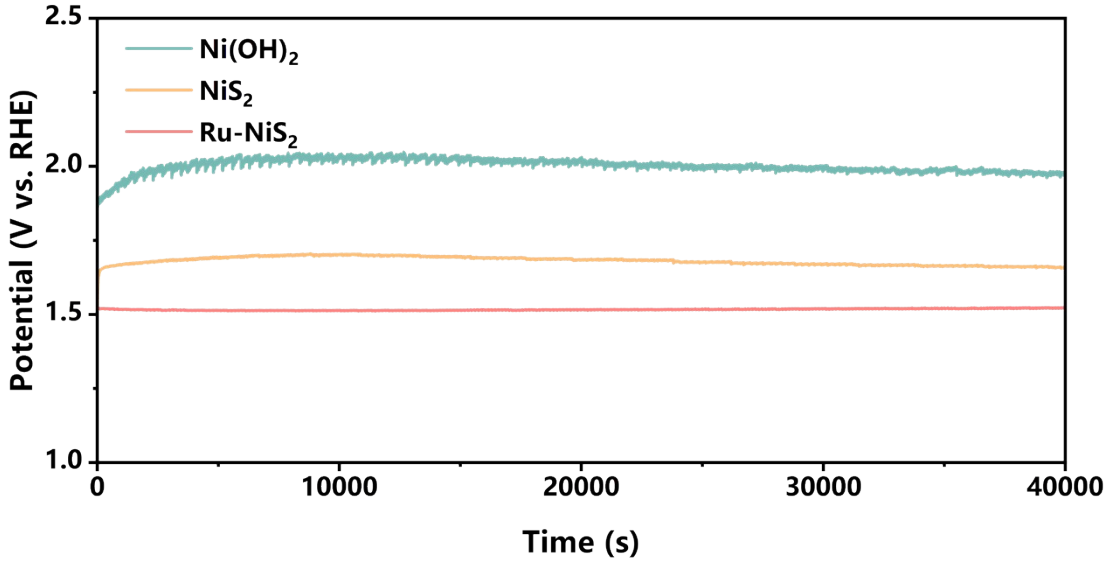

Figure S14. Galvanostatic measurement for $Ni(OH)_2$, NiS_2 and Ru-NiS_2 at the current density of 10 mA cm^{-2}.

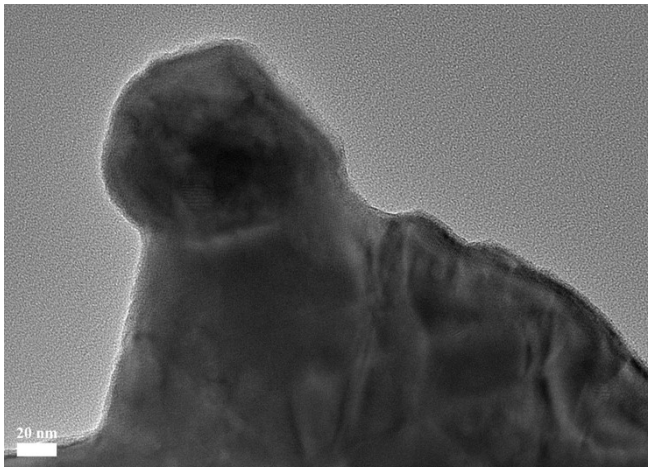

Figure S15. TEM image of Ru-NiS_2 after Galvanostatic measurement.

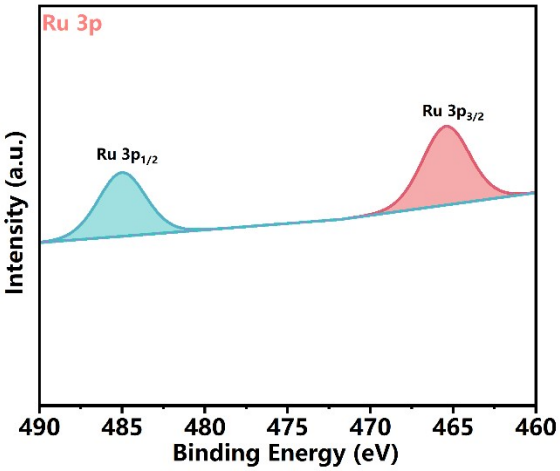

Figure S16. Ru 3p XPS spectra of Ru-NiS_2 after Galvanostatic measurement.

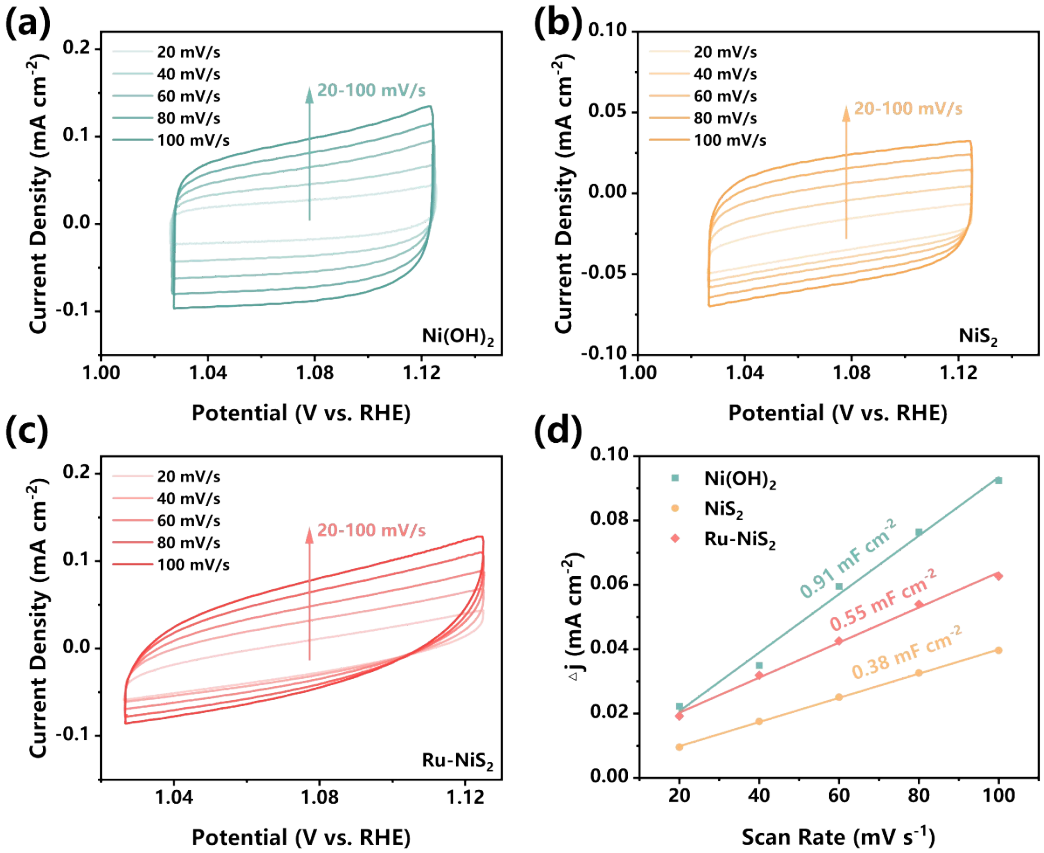

Figure S17. CV profiles of (a) $Ni(OH)_2$, (b) NiS_2 and (c) Ru-NiS_2 at different scan rates of 20, 40, 60,80, and 100 mV s^{-1}; (d) Liner fitting of the capacitive currents of the catalysts versus scan rate of the NiS_2, Ru-NiS_2, and $Ni(OH)_2$ electrocatalysts.

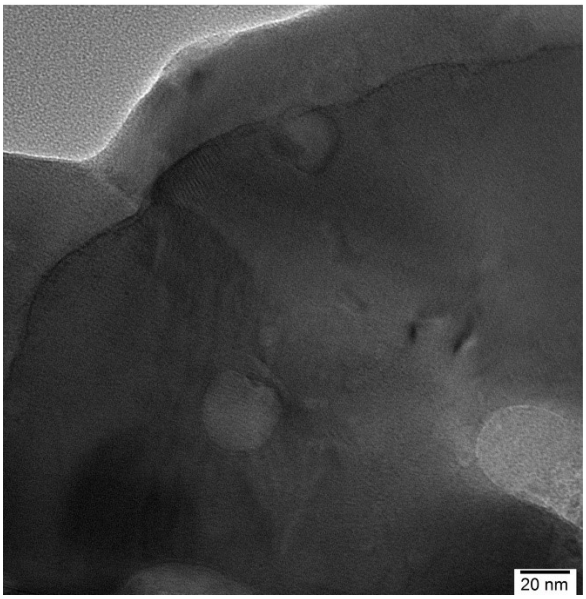

Figure S18. TEM image of Ru-NiS_2 after Long-term stability test.

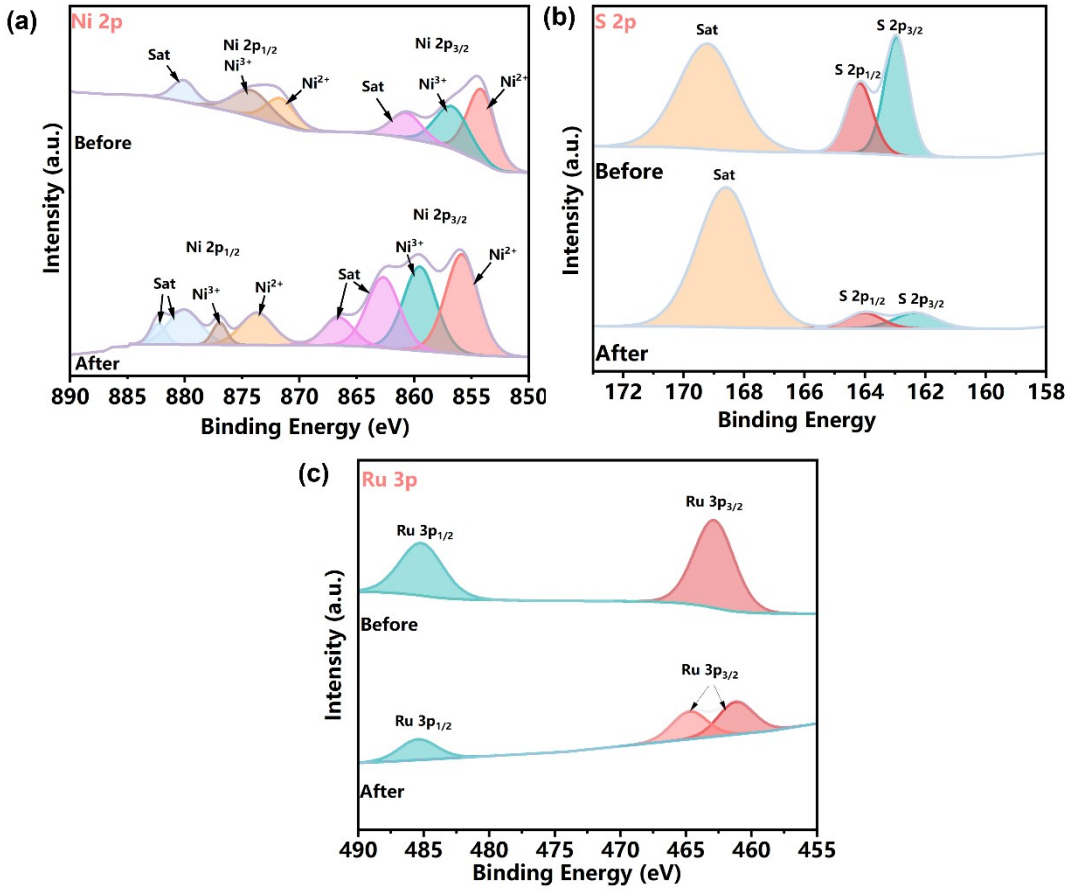

Figure S19. (a) Ni 2p, (b) S 2p and (c) Ru 3p XPS spectra of Ru-NiS2 before and after long-term stability test.

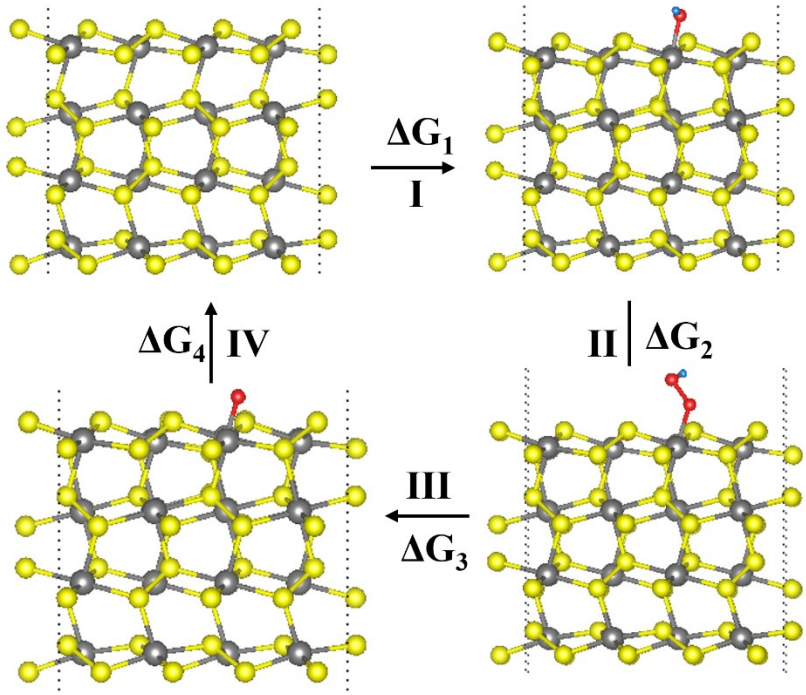

Figure S20. Established model of adsorption process with NiS_2 and oxygen containing species.

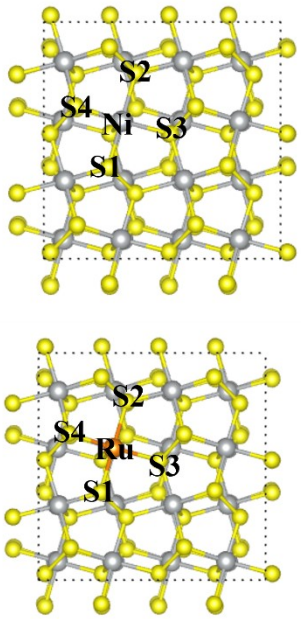

Sample	Atoms	Bader electrons	ΔQ
NiS_2	S1	6.25	0.25
	S2	6.27	0.27
	S3	6.24	0.24
	S4	6.29	0.29
	Ni	9.49	-0.51
Ru-NiS_2	S1	6.23	0.23
	S2	6.29	0.29
	S3	6.24	0.24
	S4	6.29	0.29
	Ru	7.48	-0.52

Figure S21. Bader charge analysis of NiS_2 and Ru-NiS_2.

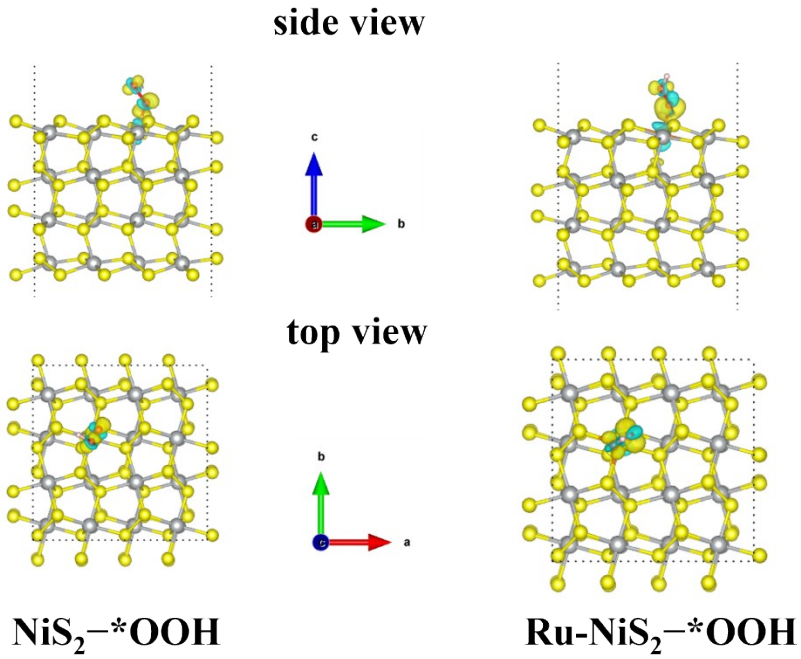

Figure S22. The charge density difference plots for *OOH on NiS_2 and Ru-NiS_2 with an isosurface value of 0.006 e·Å^{-3}.

Table S5. Comparison of the catalytic activity for OER in alkaline environments between Ru-NiS_2 and previously reported representative catalysts.

Catalysts	η@ j10 mV @10 mA cm^{-2}	Tafel slope mV dec^{-1}	Electrolytes	Reference
Ru-NiS_2	269	92	1 M KOH	This work
NiS_2	392	185	1 M KOH	This work
Co/P NF	306	51.1	1 M KOH	[5]
Co/Mo_2C	366	59.1	1 M KOH	[6]
Fe/Ni–N_x@$FeNi_3$	251	34.63	1 M KOH	[7]
RuO_2/MoO_3	267	147	0.1 M $HClO_4$	[8]
Mo-Ag	330	75	1 M KOH	[9]
MoS_2	383	96.98	1 M KOH	[10]
Au-CuO_X	380	73	1 M Na_2CO_3	[11]
$Co_{1-x}S/CoS_2$-2	310	121	0.1 M KOH	[12]
Ir-IrO_2/C	264	63.2	0.5 M H_2SO_4	[13]
CoSe	250	56	1 M KOH	[14]
CuCo-MOF/MoS_2	336	75	1 M KOH	[15]
$CoFePO_4$	285	53	1 M KOH	[16]
NiO/$CuFe_2O_4$	297	63	1 M KOH	[17]
CoNiO@NCNT	315	63.6	1 M KOH	[18]
$LaCo_{1-x}Zn_xO_3$	327	92	1 M KOH	[19]
Ir-Cu/C	311	77.3	1 M KOH	[20]

Co_3O_4	328	71	1 M KOH	[21]
Fe-$NiSe_2$	277	88.4	1 M KOH	[22]
C-$S_{0.75}$ -HT-C_{800}	277	70	1 M KOH	[23]
Bi_2-Co_8-BO_3	325	37	1 M KOH	[24]
$FeMn_2O_4$-Q	350	100.7	1 M KOH	[25]
$Ni(OH)_2$	523	190	1 M KOH	This work

Reference

[1]B. Ravel and M. Newville, *Journal of Synchrotron Radiation.*, 2005, **12** (4), 537.

[2]S. I. Zabinsky, J. J. Rehr, A. L. Ankudinov, R. C. Albers and M. J. Eller, *Physical Review B.*, 1995, **52** (4), 2995.

[3]Y. W. Wang, W. Tian, J. Wan, Y. N. Zheng, H. J. Zhang and Y. Wang, *Journal of colloid interface science.*, 2023, **645**, 833.

[4]V. Wang, N. Xu, J. C. Liu, G. Tang and W. T. Geng, *Computer Physics Communications.*, 2021, **267**, 108033.

[5]M. Yao, H. Hu, B. Sun, N. Wang, W. C. Hu and S. Komarneni, *Small.*, 2019, **15** (50), 1905201.

[6]S. F. Cui, M. Li and X. J. Bo, *International Journal of Hydrogen Energy.*, 2020, **45** (41), 21221.

[7]Y. C. Dong, Q. Liu, C. Y. Qi, G. Q. Zhang, X. D. Jiang and D. Q. Gao, *Chemical Communications.*, 2022, **58** (90), 12592.

[8]W. Q. Ren, K. X. Wang, D. Lu and C. X. Xu, *ACS Applied Energy Materials.*, 2023, **6** (24), 12573.

[9]F. A. Medeiros, R. A. Raimundo, C. S. Loureno, T. R. Silva, N. T. Cmara, A. J. M. Araújo, M. A. Morales, D. A. Macedo, U. U. Gomes and F. A. Costa, *Journal of Physics and Chemistry of Solids*., 2023, **172**, 111041.

[10]P. Joshi, S. Upadhyay and A. Pandey, *FlatChem.*, 2023, **41**, 100543.

[11]J. Y. Zhang, B. Guo, J. Liang, L. Zou, J. Lu and J. X. Liu, *ACS Applied Nano Materials.*, 2022, **5** (5), 6500.

[12]L. X. Qiao, T. Li, Z. H. Cheng, K. Y. Liu, Z. H. Chen, J. Wu, J. Lin, J. Chen, R. H. Zhu and H. Y. Yang, *Journal of Electroanalytical Chemistry.*, 2022, **918**, 116454.

[13]M. Wang, W. X. Zhu, M. J. Ma, Z. L. Fan, J. J. Yang, F. Liao and M. W. Shao, *ChemElectroChem.*, 2022, **9** (19), e202200732.

[14]M. Bilal, Rashid, A. Altaf, N. Baig, G. A. Chotana, R. S. Ashraf, S. Rasul, A. Nafady, A. Ul-Hamid and M. Sohail, *Fuel: A journal of fuel science.*, 2022, **323**, 124324.

[15]Q. Li, X. B. Hu, L. D. Zhang, S. Y. Li, J. Y. Chen, B. Y. Zhang, Z. Y. Zheng, H. Y. He, J. Zhang, S. P. Luo and A. J. Xie, *Electrocatalysis.*, 2022, **14** (3), 333.

[16]S. Manzoor, A. G. Abid, S. Aman, M. Abdullah, A. R. Rashid, H. M. Ali, T. E. Ali, M. A. Assiri, M. N. Ashiq and T. A. Taha, *Ceramics International.*, 2022, **48** (24), 36975.
[17]A. BaQais, M. Shariq, E. Almutib, N. Al-Qasmi, R. E. Azooz, S. K. Ali, K. F. Hassan and M. Iqbal, *The European Physical Journal Plus.*, 2023, **138** (9), 804.
[18]T. Zhao, Z. R. Song, X. Wang and J. K. Gao, *Journal of Solid State Chemistry.*, 2023, **326**, 124213.
[19]F. Hadji, M. Omari and M. Mebarki, *Ceramics International.*, 2023, **49** (15), 25405.
[20]W. X. Zhou, P. N. He, A. D. Wu, Y. Y. Wang, Y. Shuai, T. Zhang, S. C. Liu and Y. Liu, *Chemical Communications.*, 2023, **59** (75), 11260.
[21]R. A. Raimundo, C. S. Lourenço, N. T. Câmara, T. R. Silva, J. R. D. Santos, A. J. M. Araújo, M. M. S. Silva, J. F. G. d. A. Oliveira, D. A. Macedo and U. U. Gomeset al, *Journal of Electroanalytical Chemistry.*, 2023, **932**, 117218.
[22]W. C. Zhuang, M. L. Du, X. H. Lu, Z. Y. Chen, Z. J. Huang, D. S. Liu, W. J. Cheng and L. Tian, *Ionics.*, 2023, **29** (3), 1069.
[23]H. Y. Li, N. Li, P. P. Zuo, S. J. Qu, F. F. Qin and W. Z. Shen, *Journal of Colloid and Interface Science.*, 2023, **640**, 391.
[24]B. Thomas, C. Tang, M. Ramírez-Hernández and T. Asefa, *ChemPlusChem.*, 2023, **88** (5), e202300104.
[25]C. Y. Qi, Q. Liu, Y. C. Dong, G. Q. Zhang, X. D. Jiang and D. Q. Gao, *Journal of Alloys and Compounds.*, 2023, **967**, 171754.